Synthesis of CeO2@SiO2 core–shell nanoparticles by water-in-oil microemulsion. Preparation of functional thin film

Fabien Grasset, R. Marchand, A.-M. Marie, D. Fauchadour, F. Fajardie

Elsevier Editorial System(tm) for Journal of Colloid And Interface Science

Manuscript Draft

Manuscript Number: JCIS-06-25R2

Title: Synthesis of CeO2@SiO2 Core-Shell Nanoparticles by Water-in-Oil Microemulsion. Preparation of Functional Thin Film.

Article Type: Regular Article

Section/Category: D. Fine Particles, Colloid Materials, and Colloid Stability

Keywords: Nanocolloids, Microemulsion, DLS, CeO2, Silica, Core-shell, Nanoparticles

Corresponding Author: Dr. Fabien Grasset, PhD

Corresponding Author's Institution: Sciences Chimiques de Rennes

First Author: Fabien Grasset, PhD

Order of Authors: Fabien Grasset, PhD; Roger Marchand, PhD; Anne-Marie Marie, PhD; David Fauchadour, PhD; Franck Fajardie, PhD

Manuscript Region of Origin:

Abstract: Synthesis of nanoparticles under restricted environment offered by water-in-oil (W/O) microemulsions provides excellent control over particle size and shape, and inter-particle spacing. Such an environment has been involved to synthesize silica nanoparticles with a CeO2 core, so-called CeO2@SiO2. Aqueous fluids made up of ceria nanoparticles with a size close to 5 nm have been used as the water phase component. The starting CeO2 sols and obtained CeO2@SiO2 nanoparticles have been characterized by Dynamic Light Scattering (DLS), X-ray diffraction, scanning and transmission electron microscopy, and specific surface area measurements. The microemulsion process has been characterized by DLS. Preliminary results on CeO2@SiO2 thin films are presented.

Synthesis of CeO_2@SiO_2 Core-Shell Nanoparticles by Water-in-Oil Microemulsion. Preparation of Functional Thin Film.

F. GRASSET[a], R. MARCHAND[a], A.-M. MARIE[b], D. FAUCHADOUR[c], F. FAJARDIE[c]

[a] UMR « Science Chimiques de Rennes » UR1-CNRS 6226, Groupe Chimie du Solide et Matériaux, Université de Rennes 1, Campus de Beaulieu, CS74205, F-35042 Rennes Cedex (France)

[b] Institut des Matériaux Jean Rouxel (IMN), UMR 6502, 2 rue de la Houssinière, BP 32229, F-44322 Nantes Cedex 03 (France)

[c] RHODIA Recherches, 52 rue de la Haie Coq, F-93300, Aubervilliers (France)

Address:
Dr. Fabien GRASSET
UMR UR1-CNRS 6226, Sciences Chimiques de Rennes
Equipe Chimie du Solide et Matériaux
Université de Rennes 1
CS 74205
35042 Rennes CEDEX
FRANCE
Telephone: +33 (0)2 23 23 65 40
Fax: +33 (0)2 23 23 56 83
grasset@univ-rennes1.fr

Abstract

Synthesis of nanoparticles under restricted environment offered by water-in-oil (W/O) microemulsions provides excellent control over particle size and shape, and inter-particle spacing. Such an environment has been involved to synthesize silica nanoparticles with a CeO_2 core, so-called $CeO_2@SiO_2$. Aqueous fluids made up of ceria nanoparticles with a size close to 5 nm have been used as the water phase component. The starting CeO_2 sols and obtained $CeO_2@SiO_2$ nanoparticles have been characterized by Dynamic Light Scattering (DLS), X-ray diffraction, scanning and transmission electron microscopy, and specific surface area measurements. The microemulsion process has been characterized by DLS. Preliminary results on $CeO_2@SiO_2$ thin films are presented.

Keywords: Nanocolloids, Microemulsion, DLS, CeO_2, Silica, Core-shell, Nanoparticles

CeO_2-based materials have attracted considerable attention from both scientific and technological point of view (examples of commercial products: Anti-UV: RHODIGARD™; catalysis: EOLYS®…). Particularly, CeO_2 nanoparticles have generated a large research effort in the past twenty years[1-21]. If a large number of reports can be found on the synthesis of CeO_2 nanoparticles, there are only a few dealing with surface modification. Recently, the nanostructured SiO_2-CeO_2 system has become very popular for chemoselective catalysis thanks to the fact that the mineral binder SiO_2 is able to generate high specific surface area and thermal stability in nanoparticles arrays[22-27]. In the case of coating oxide particles with silica, various routes have been investigated: aggregation of small colloids[28], condensation of silica oligomers produced by solubilization of silica particles in highly basic medium[29], hydrolysis of functionalized or not silicon alkoxides[22-27, 30-33], microemulsion route[34-37].

In this study, the water-in-oil (W/O) microemulsion route was chosen because it provides a unique environment to synthesize novel inorganic materials with interesting designs and/or specific properties[34], resulting in non-aggregated nanoparticles with a controlled surface and/or coating properties. Nevertheless, at present, a major problem with the microemulsion process remains the effect of the reactants and products on the microemulsion stability domain, particularly the metal concentration in the aqueous pseudo-phase used for precipitation reactions[27,34]. That is why, avoiding the classical precipitation process, we describe in this paper an original method to synthesize designed nanoparticles using a colloidal suspension as the starting water pseudo-phase[35,36]. This colloidal suspension allows the metal concentration to be increased without destabilizing the microemulsion, and to avoid the classical calcination process[27]. The present work aimed at obtaining well designed and characterized core-shell CeO_2@SiO_2 nanoparticles, as well as more information about the W/O microemulsion process.

1 Experimental

1.1 Products

Two CeO_2 sols (A and B) were provided by Rhodia laboratory. The surface chemistry informations are described in ref. 20 and 21. The pH values ranged from 1.1 to 2, the CeO_2 concentration from 10 to 100 g/L and the viscosity from 1.12 to 1.45 mPas. All the reagents were of 99% min. purity, they were used without further purification: Acetone, ethanol, n-heptane, aqueous ammonia solution (28%), tetraethoxysilane (TEOS). Sulfosuccinic acid bis [2-ethylhexyl] ester sodium salt (AOT) and polyoxyethylene(4) lauryl ether (Brij30) were provided from Aldrich Chemical Co. Those AOT and Brij30 surfactants were selected for this study because at room temperature they are readily soluble in saturated hydrocarbons like n-heptane.

1.2 Synthesis of CeO_2@SiO_2 core-shell nanoparticles and thin films

n-heptane was used as the oil phase component of the microemulsion, with different amounts of AOT/Brij 30 mixture and aqueous phase (Table 1). The weight ratio between AOT and Brij30 was 1. The aqueous phase contained the CeO_2 sol, TEOS and aqueous ammonia solution. In more detail, the microemulsion (noted 1 or 2 using the sol A or B, respectively) was prepared by adding acidic CeO_2 sol into a surfactant/heptane mixture. Then, TEOS as the precursor of silica nanoparticles was added to the microemulsion. Finally, ammonia solution was carefully added for the condensation of TEOS. In the case of Brij 30, in order to avoid any complications due to the presence of a possible thermally induced phase inversion, the reaction temperature was kept below 25°C. After 48 h, all the samples were washed with n-heptane, ethanol and acetone to remove surfactant and oil, and a separation followed in a centrifuge at 5000 rpm for 15 min. The resulting powders were dried at 60°C under vacuum. Concerning wet films prepared from the microemulsion solutions via dip coating of glass slides, they were pre-sintered at 400°C in air to remove organic residues.

1.3 UV-vis spectra

UV-vis spectra of the colloids were recorded with a Varian CARY 5 spectrometer.

1.4 Dynamic Light Scattering (DLS)

To determine the mean hydrodynamic diameter (d(H)) of the nanocrystals or nanodroplets, DLS investigations on microemulsions or sols were performed with a Zetasizer Nano ZS from Malvern Instruments with the new non-invasive back scatter (NIBS) technology. The DLS technique measures the particle or droplet diffusion due to Brownian motion and relates it to the particle size. The particle size is classically calculated by using the Stokes-Einstein equation $d(H)=\frac{kT}{3\pi\eta D}$ where D is the translational diffusion coefficient, k the Boltzmann's constant, T the absolute temperature and η the viscosity. As can be seen from the Stokes-Einstein equation, there is a direct relationship between viscosity and particle size. The viscosity required for this technique is the dynamic viscosity of the sample at zero shear rate and the accuracy of the determined particle size is directly related to that of the viscosity. The viscosity of the sols A and B was measured with the viscosimeter SV10 from Malvern.

1.5 X-ray intensity measurements

X-ray diffraction data were recorded at room temperature on a Philips PW 3020 using the Bragg-Brentano geometry with CuKα radiation (40kV, 30mA, integration time range from 0.5 s to 10 s) and a secondary monochromator. The average apparent crystallite size (ε_β) was evaluated from a whole diffraction pattern profile analysis, using last developments implemented in the Fullprof program (version 2.0 Nov 2001, LLB, Juan Rodriguez-Carvajal). By description of instrumental and intrinsic profiles by normalized Voigt function (convolution of gaussian and lorentzian functions), size and strain effects can be separated from the whole profile analysis based on the different angular dependence of the gaussian and

lorentzian Full-Width-at-Half-Maximum (H_G and H_L respectively), according to the following equations

$$H_G^2=(U_{strain\_iso}+(1-\xi)D^2_{strain\_aniso})tg^2\theta+\frac{G_{size\_iso}}{\cos^2\theta}$$

$$H_L=(X_{strain\_iso}+\xi D_{strain\_aniso})tg\theta+\frac{Y_{size\_iso}+F_{size\_aniso}}{\cos\theta}$$

where U, X, ξ, G and Y are refinable parameters, and D and F are analytical functions (which depend on a set of additionable refinable parameters) to model the hkl-dependent broadening due to strain and size effects, respectively. "Perfect" Y_2O_3 powder was used as a standard to determine the Instrumental Resolution Function (IRF) of the diffractometer. The observed line broadening was modeled by isotropic size effects, leading to $1/\cos\theta$ dependent terms of H_G and H_L (Y and G parameters in Fullprof, respectively) contribution to the size effects. Refinement of $tg\theta$ dependent isotropic strain parameters (U and X parameter in Fullprof) did not improve significantly the profile fitting. For each diffraction pattern, a counter zero point and the unit-cell parameters were refined in addition to the Y and G parameters. The background level was defined by a polynomial function. After refinement of the coefficients, the program calculates the apparent size along each reciprocal lattice vector. The average apparent crystallite size (ε_β) can be related to the true size, but only if the crystallite shape is known or assumed. For instance, for a spherical crystallite, the true diameter D is simply derived from $4/3(\varepsilon_\beta)$. Moreover, this simple relation is strictly valid for a monodisperse system[38]. The true size could be defined only in the case of single-domain nanoparticles without amorphous shell, as the size estimated from Transmission Electron Microscopy (TEM) and/or Scanning Electron Microscopy (SEM) images.

1.6 Morphological investigations by SEM and TEM

SEM photographs by JEOL JSM 6301F were taken to examine the shape and size of the silica.nanoparticles

A transmission electron microscope (Hitachi H 9000 Nar operating at 300 kV) was used to study the shape and size of the CeO_2@SiO_2 nanoparticles. Samples were prepared by direct deposition of dry powder dispersed in ethanol on carbon activated Cu-grids.

1.7 Specific Surface area

The BET specific surface area was determined by following the standard N_2-adsorption method, using a Micromeritics ASAP-200 instrument. The samples were degassed at 200ºC for 2h to clean the surface and the N_2 adsorption isotherms were determined at 77K.

2 Results and Discussion

2.1 CeO_2 nanoparticles

Compared UV-vis absorption spectra and DLS investigation results of the CeO_2 sols A and B are shown in Figs. 1 and 2, respectively. The sol A gives a classical UV-vis absorption spectrum without scattering whereas the sol B shows a broad spectrum relative to large particles according the Lord Rayleigh theory. Concomitantly, as can be seen in Fig. 2, the mean hydrodynamic diameter goes up from 7 nm for the sol A to around 40 nm for the sol B. Fig. 3 shows the observed, calculated and difference XRD patterns (integration time of 10 s) of a typical CeO_2 nanopowder obtained from sols A and B by increasing the pH to 7 by adding a base (NH_3 (28%) or NaOH (1M)) generating a rapid phase separation of a dense precipitate as already observed in ref 21. The diffraction peaks are broad and similar to those typically observed for nanoparticles. In all cases (A and B sols), the average grain size of the particles determined by XRD was ~ 4 nm, that is fairly consistent with TEM data reported by Nabavi et al.[20] (particle diameter about 5-6 nm).. The specific surface area measurements of

Formatted

CeO_2 nanopowders obtained from the sol A showed a high value (noted S_{BET}) of 180 $m^2.g^{-1}$. Using the relation developed by Audebrand et al.[38], the mean BET surface area diameter (noted D_{BET}) for a spherical nanoparticle is given by $D_{BET}=\frac{6x10^4}{\rho S_{BET}}$ where ρ is the theoretical density of CeO_2 (7.2 $g.cm^{-3}$). The calculated value of D_{BET} is 4.6 nm, that is fairly consistent with the XRD studies. The XRD and BET experiments enable us to show indirectly that even after the increase in the pH after NH_3 addition, the size of the nanoparticles is not modified. These results were confimed by TEM images (Figures 4 and 5). In the case of sol A, the TEM study agrees with the XRD and DLS values whereas the sol B agree only with DLS value. The sol B consisted of controlled aggregated 4 nm primary nanoparticles (Fig. 5).

2.2 CeO_2@SiO_2 core-shell nanoparticles

As mentioned above, the silica nanoparticles with a CeO_2 core were prepared by a low temperature water-in-oil (W/O) microemulsion technique. Microemulsions are defined as clear thermodynamically stable dispersions of two immiscible liquids containing appropriate amounts of surfactant[34]. A W/O microemulsion consists of an oil phase, a water phase and surfactant, with specific physico-chemical properties such as transparency, isotropy and thermodynamic stability[34]. In our process we used directly a colloidal suspension as a pseudo-phase in order to increase the metal concentration without destabilizing the microemulsion. The concentration of CeO_2 can easily reach 25% in the CeO_2@SiO_2 core-shell nanoparticles without destabilizing the microemulsion and avoid the classical calcination process to compare with the method (17%) to use by tago[27]. Moreover, two kinds of surfactant were used, accrediting the commonly considered fact that the presence of two different surfactants at the interface between water and oil phases gives a lower interfacial tension. Bidyut K. Paul et al (ref 39) show that the addition of Brij30 in AOT/IPM reverse micellar systems induces synergism in solubilization of water. The produced optical transparency upon vigorous

stirring indicated formation of a stable microemulsion. After TEOS addition into the surfactant/heptane/sol mixture, the silica shell was synthesized by increasing the pH inside the droplets with ammonia solution that catalyzes the TEOS condensation. Once all the products added, the microemulsion was keeping clear for few days. Preliminary measurements by DLS of the droplet size distribution in the microemulsion 1 are reported in Fig. 6. A scattering technique was used to determine the droplet size, however, it should be noted that, although this technique provides a good indication of size in the case of relatively dilute solutions, interpretation is more difficult when a concentrated system is studied, because of interactions between individual particles[40]. Microemulsions were typically prepared at high concentrations because dilution frequently changes the microstructure, and even induces disappearance of the droplets[34]. As indicated above, the use of the dynamic viscosity at zero shear rate gives a size independent on concentration. Surprisingly, in spite of approximations (no correction of the interparticulate interaction and use of the viscosity of heptane instead of the real value), the size obtained by DLS (Figs 6a and b) corresponds to that determined for CeO_2 sol (Sol A Fig. 2). This d(H) value (7 nm) of CeO_2 nanoparticles (Figs. 2 and 6a, b) was used as a "reference" to assume that the value equal to 40-45 nm corresponds to the hydrodynamic diameter of the droplets. As can be seen in Fig. 6b, addition of TEOS (without ammonia) did not change very much the microstructure of the microemulsion (even after 24h, d(H) = 45 nm), whereas after the ammonia addition, the droplet size followed the expected trend, i.e. an increase (d(H) = 140 nm after 24h) with increasing the water volume fraction and formation of silica nanoparticles. Disappearance of the d(H) of CeO_2 confirmed the presence of silica nanoparticles in the droplets. We can explain the low modification of TEOS during the first 24h by the fact that TEOS is an organophilic molecule which, therefore, is more readily dissolved in heptane than in aqueous droplets. Nevertheless, in our case, adapting the work of Arriagada *et al.*[41], the hydrolysis of TEOS should be catalyzed by the acid sol initially present

in the droplets. Indeed, the $Si(OC_2H_5)$ groups are protonated under such conditions, making alcohol a better leaving group and increasing, therefore, the hydrolysis kinetics. The hydrolysis reaction generates Si(OH) groups according to:

$$Si(OC_2H_5)_4 + m\ H_2O \rightarrow Si(O\ C_2H_5)_{4-m}(OH)_m + m\ C_2H_5OH.$$

Those Si(OH) groups should be involved in the base-catalyzed condensation step, inducing formation of Si-O-Si or Si..OH..Si bonds via olation, oxolation or alcoxolation[34,41]. According to ref. 40, we assume that the main part of the TEOS monomeric species was only hydrolyzed after 48h and, consequently, had already migrated into the droplets before condensation and formation of SiO_2.

In Fig. 7, comparison between XRD (integration time of 0.5 s) powder patterns of CeO_2@SiO_2 core-shell and CeO_2 nanoparticles shows that the broad diffraction peaks for $15° < 2\theta < 33°$ are relative to amorphous silica. As expected, the peaks assigned to CeO_2 are observed with right relative intensities. As already reported in the microemulsion synthesis of $ZnFe_2O_4$-silica core-shell nanoparticles[37], the specific surface area of the CeO_2@SiO_2 nanoparticles lay in the range 80-150 $m^2.g^{-1}$. These relatively high values regarding the silica particle size mean porous particles due probably to not condensed silanol groups. SEM micrographs of core-shell powders prepared from different sols and/or surfactants are presented in Fig. 8 (a and b for the microemulsions 1 and 2, respectively). In all cases the silica nanoparticles consisted of an arrangement of relatively uniform particles. In microemulsion 1, the particle diameter is 30-50 nm, and 60-80 nm in microemulsion 2. The silica particle size is closely dependent on the CeO_2 core size. Figs. 4 and 5 display TEM micrographs of samples issued from microemulsions 1 and 2, respectively. The presence of CeO_2@SiO_2 core-shell nanoparticles is clearly shown. The TEM study corroborates the XRD results and confirms also the shape of the silica particles observed by SEM. The most

noticeable feature in Fig. 5 (microemulsion 2) is the location of the CeO_2 nanocharge at the center of the spherical silica particle. The TEM and SEM studies demonstrate that the shape of the nano-reactor can be completely controlled in order to obtain spherical silica nanoparticles with embedded a single CeO_2 charge of intermediate size.

From CeO_2@SiO_2 microemulsions we have succeeded to prepare functional thin films on conventional glass and SiO_2 substrats via dip-coating. Fig. 9 illustrates a CeO_2@SiO_2 core-shell nanoparticles thin film elaborated from microemulsion 2. The film was annealed in air at 400°C for 15 min. UV-vis spectra and a study of mechanical properties of different CeO_2@SiO_2 thin films are now in progress. Preliminary results evidence the central role played by the particle habitat. Moreover, a recent study of the mechanical properties of a pure silica nanoparticles 50 nm thin film (synthesized by W/O microemulsion) coating commercial soda lime silicate glass shows an improvement of the glass surface properties[42]. In fact, the silica nanoparticles are found to spread out the stress at the surface/indenter contact and to favor a microductile behavior.

3 Conclusion

By using a microemulsion process, it has been possible to prepare spherical silica nanoparticles with a CeO_2 core. They have been elaborated by a low temperature water-in-oil microemulsion technique. The diameter of the silica particles, in the range of 30-80nm, closely depends on the CeO_2 core size. Considering our first idea, i.e. the control over the design of nanoparticles, the concept of very stable “nano-reactors” or “nano-droplets” is the essential parameter for the formation of core-shell nanoparticles. These silica nanoparticles with a CeO_2 core have potential as anti-UV thin films. Another interest lies in the formation of nanostructured materials for application in advanced catalysis, where the hierarchical

porosity combines efficient transport and high surface area. In particular, silica spheres could be used to make three-dimensional porous replicas materials.

Acknowledgements

The authors thank J. Le Lannic and N. Pontais for their valuable technical assistance. The University of Rennes 1, the CNRS and the Rhodia Company have funded this work.

References

1) Vantomme, A.; Yuan, Z.-Y.; Du, G.; Su, B.-L.; Langmuir, 21(3) (2005) 1132.

2) Shu-Hong Yu, Cölfen H. and Fischer A.; Colloids and Surfaces A: Physicochem. and Eng. Aspects, 243(1-3) (2004) 49.

3) Bumajdad, A.; Zaki, M. I.; Eastoe, J.; Pasupulety, L.; Langmuir**,** 20(25) (2004) 11223.

4) Chen H.I. and Chang H.Y.; Colloids and Surfaces A: Physicochem. and Eng. Aspects, 242(1-3) (2004) 61.

5) Wang, Z. L.; Feng, X.; J. Phys. Chem. B., 107(49) (2003) 13563.

6) Maciel A.P., Lisboa-Filho P. N., Leite E. R., Paiva-Santos C. O., Schreiner W. H., Maniette Y. and Longo E.; J. Eur. Ceram. Soc., 23(5) (2003) 707.

7) Yongjun H., Bolun Y. and Guangxu C.; Mater. Let., 57(13-14) (2003) 1880.

8) Yin L., Wang Y., Pang G., Koltypin Y. and Gedanken A.; J. Colloid Interface Sci., 246(1), (2002) 78.

9) Wu, Z.; Zhang, J.; Benfield, R. E.; Ding, Y.; Grandjean, D.; Zhang, Z.; Ju, X.; J. Phys. Chem. B., 106(18) (2002) 4569.

10) Zhang F., Chan S., Spanier J.E., Apak E., Jin Q., Robinson R.D. and Herman I.P.; Applied Phys. Lett., 80(1) (2002) 127.

11) Hirano M., Miwa T. and Inagaki M.; J. Solid State Chem., 158(1) (2001) 112.

12) Zhang, J.; Ju, X.; Wu, Z. Y.; Liu, T.; Hu, T. D.; Xie, Y. N.; Zhang, Z. L.; Chem. Mater., 13(11) (2001) 4192.

13) Wu Z., Guo L., Li H., Yang Q., Li Q.and Zhu H.; Mater. Sci. Eng. A, 286(1) (2000) 179.

14) Tsunekawa S., Fukuda T. and Kasuya A.; Applied Surface Sci., 457(3) (2000) L437.

15) Tsunekawa S., Fukuda T. and Kasuya A.; J. Applied Phys., 87(3) (2000) 1318.

16) Bai W., Choy K.L., Stelzer N.H.J. and Schoonman J.; Solid State Ionics, 116(3-4) (2000) 225.

17) Masui T., Machida K., Sakata T., Adachi G. and Mori H.; Chem. Mater., 9 (1997) 2197

18) Masui T., Machida K., Sakata T., Mori H. and Adachi G.; J. Alloys Comp., 256 (1997) 97.

19) De Fariaand L.A., Trasatti S.; J. Colloid Inter. Sci., 167 (1994) 352.

20) Nabavi M., Spalla O. and Cabane B.; J. Colloid Interface Sci., 160 (1993) 459.

21) Sehgal A., Lalatonne Y., J.F. Berret and Morvan M., Langmuir, 21 (2005) 9359.

22) Chane-Ching J. Y., Airiau M., Sahibed-dine A., Daturi M., Brendle E.; Ozil F., Thorel A., Corma A.; Langmuir, 21(4) (2005) 1568.

23) Reddy B. M., Khan A., Lakshmanan P., Aouine M., Loridant S., Volta J.-C.; J. Phys. Chem. B., 109(8) (2005) 3355.

24) Concepcion P., Corma, A.; Silvestre-Albero, J.; Franco, V.; Chane-Ching, J. Y.; J. Am. Chem. Soc., 126(17) (2004) 5523.

25) Corma A., Chane-Ching J.Y., Airiau M. and Martínez C.; J. Catal., 224(2) (2004) 441.

26) Cui H., Hong G., Wu X. and Hong Y.; Mater. Res. Bull., 37(13) (2002) 2155.

27) Tago T., Tashiro S., Hashimoto Y., Wakabayashi K. and Kishida M.; J. Nanoparticle Res., 5 (2003) 55.

28) Homola A. P., Lorentz M.R., Suusner H., Rice S.; J. Applied Phys. 61 (1987) 3898.

29) Philips A.P., Van Brugge M.P.B. and Pathmamanoharan C.; Langmuir, 10 (1994) 92.

30) Klotz M., Ayral A., Guizard C., Ménager C., Cabuil V.; J. Colloid Inter. Sci., 220 (1999) 357.

31) Grasset F., Saito N., Li D., Park D.C., Sakaguchi I., Ohashi N., Haneda H., Roisnel T., Mornet S. and Duguet E.; J. Alloys Comp., 360 (2003) 298.

32) Grasset F., Mornet S., Duguet E., Demourgues A., Portier J., Bonnet J. and Vekris A.; J. Magn. Magn. Mater., 234 (2001) 409.

33) Mornet S., Vasseur S., Grasset F. and Duguet E.; J. Mater. Chem., 14 (2004) 2161.

34) Kumar P. and Mittal K.L., Handbook of Microemulsion Science and Technology, by Marcel Dekker, Inc., New-York, 1999.

35) Tago T., Nagase R., Hatsuta T., Kishida M. and Wakabayshi K.; Proc. 8th Int. Conf. on Ferrites, ICF8, Kyoto 2000, (2001) 763.

36) Mornet S, Grasset F, Duguet E, and Portier J.; Proc. 8th Int. Conf. on Ferrites, ICF8, Kyoto 2000, (2001) 766.

37) Grasset F., Labhsetwar N., Li D., Park D.C., Saito N., Haneda H., Cador O., Roisnel T., Mornet S., Duguet E., Portier J., Etourneau J.; Langmuir, 18 (21) (2002) 8209.

38) Audebrand N., Auffrédic J.P., Louër D.; Chem. Mater., 10 (1998) 2540.

39) Bidyut K. Paul and Rajib K. Mitra, J. Colloid Interface Sci, 288, 1 (2005) 261.Aboofazeli R., Barlow D.J., Lawrence M.J.; AAPS Pharm. Sci., 2(2) (2000) 19.

41) Arriagada F. J., Osseo-Asare K.; Colloids Surf. A: Physicochem. Eng. Aspects, 154 (1999) 311.

42) Tartivel R., Reynaud E., Grasset F, Sangleboeuf J.C. and Rouxel T., Nanoletters, submitted.

Figure captions

Fig.1: UV-vis absorption spectra of sols A and B.

Fig. 2: DLS investigations of sols A and B.

Fig. 3: Observed (dots), calculated (full line) and difference X-ray powder diffraction profiles of typical CeO_2 nanopowders obtained from sols A and B.

Fig. 4: TEM micrograph of $CeO_2@SiO_2$ nanoparticles resulting from microemulsion 1.

Fig. 5: TEM micrograph of $CeO_2@SiO_2$ nanoparticles resulting from microemulsion 2.

Fig. 6: DLS investigations of microemulsion 1. a : heptane/surfactant/CeO_2 sol system; b: heptane/surfactant/CeO_2 sol/TEOS system; c: heptane/surfactant/CeO_2 sol/TEOS/ammonia system.

Fig. 7: XRD patterns of $CeO_2@SiO_2$ core-shell (A) and CeO_2 (B) nanoparticles.

Fig. 8: SEM images of $CeO_2@SiO_2$ core-shell nanoparticles (A and B corresponding to microemulsions 1 and 2, respectively).

Fig. 9: SEM image of a $CeO_2@SiO_2$ thin film elaborated from microemulsion 2 by dip-coating.

Table caption

Table 1: Experimental preparation conditions of the microemulsions 1 and 2.

Table

	Heptane (wt%)	Surfactants (wt%)	Aqueous phase (wt%) (H_2O/TEOS/NH_3)
Microemulsion 1	63.5	27.5	3.2/3.7/2.1
Microemulsion 2	63.1	27.6	3.2/3.8/2.3

Figure

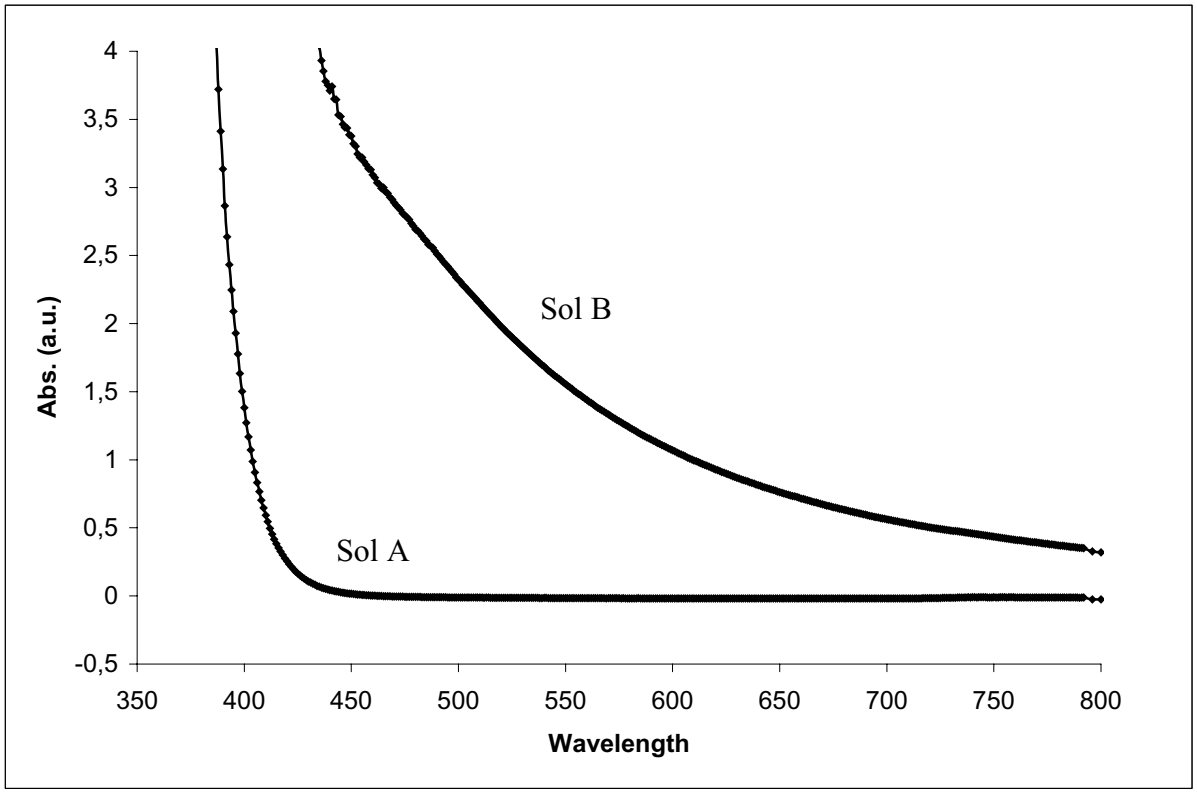
4
3,5
3
2,5
2
1,5
1
0,5
0
-0,5
Abs. (a.u.)
Sol B
Sol A
350
400
450
500
550
600
650
700
750
800
Wavelength

Figure

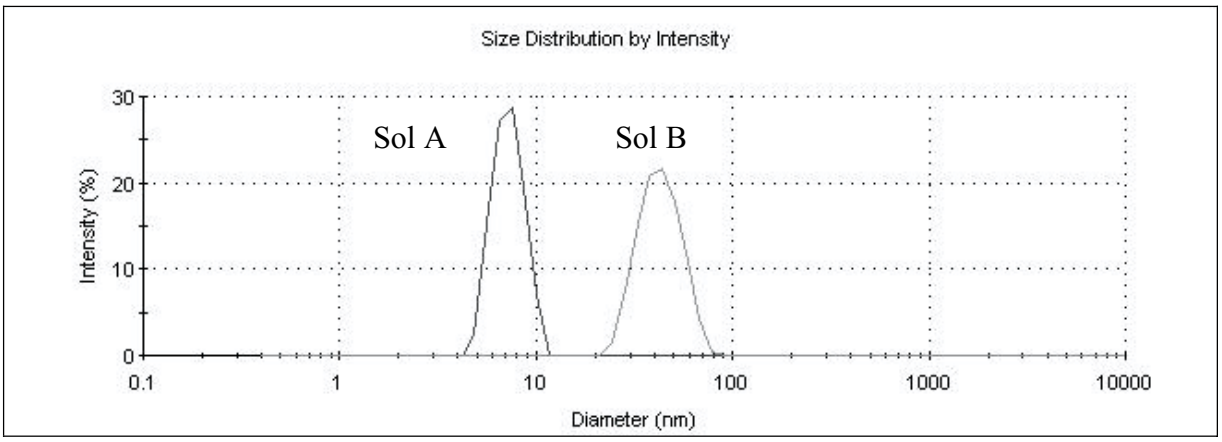
Size Distribution by Intensity
Sol A
Sol B
Intensity (%)
30
20
10
0
0.1
1
10
100
1000
10000
Diameter (nm)

Figure

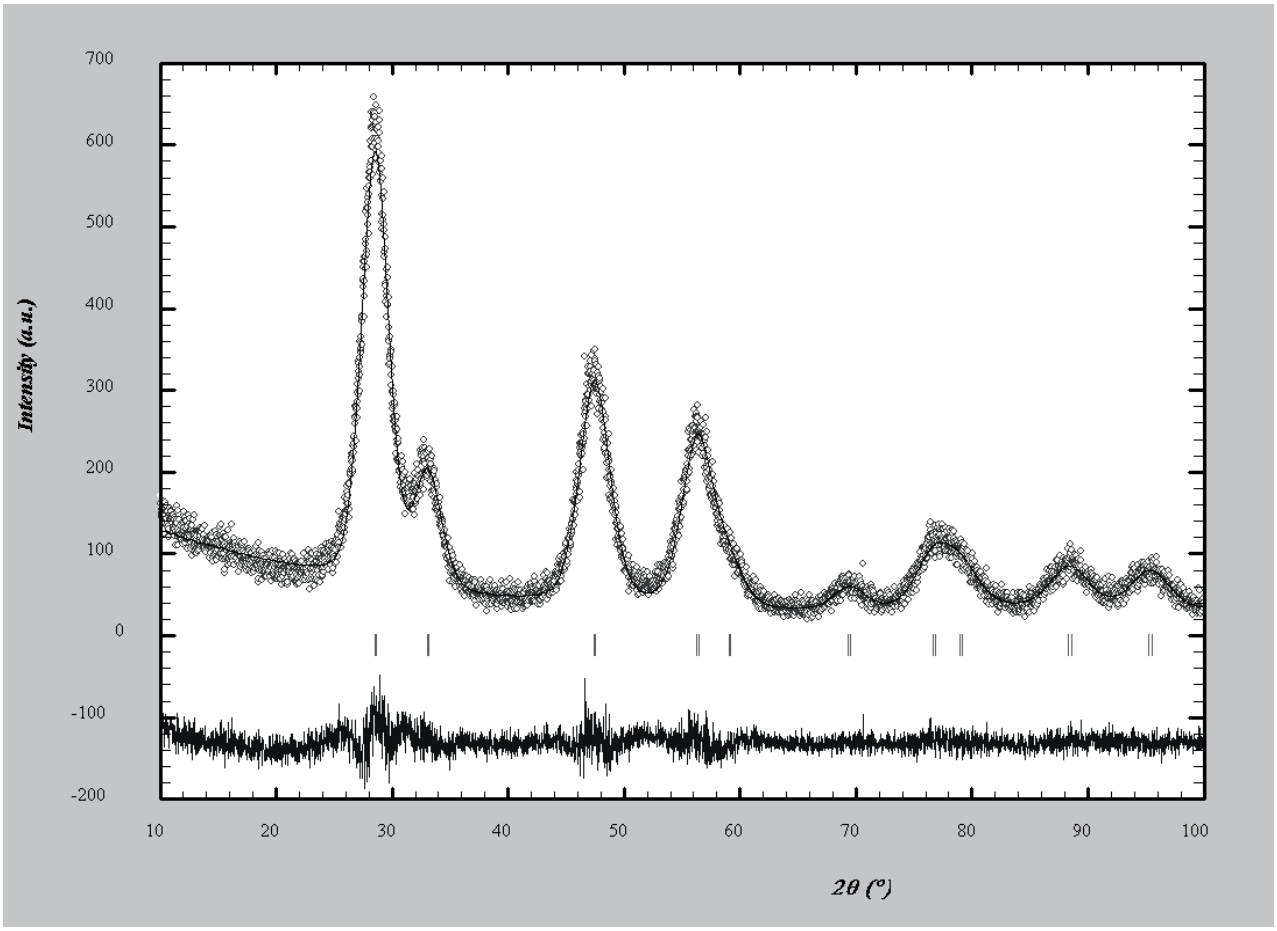
700
600
500
400
300
200
100
0
-100
-200
Intensity (a.u.)
10
20
30
40
50
60
70
80
90
100
2θ (°)

Figure

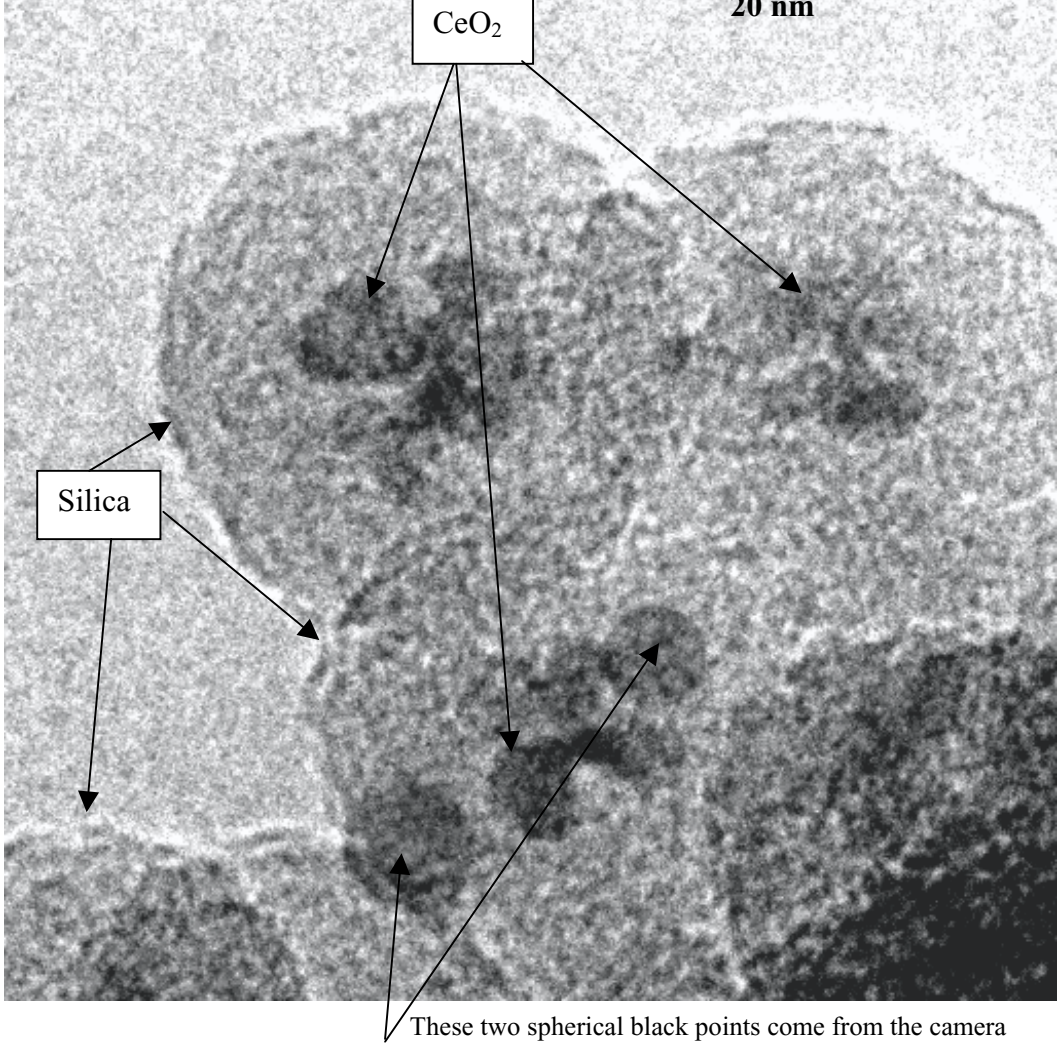
20 nm
CeO_2
Silica
These two spherical black points come from the camera

Figure

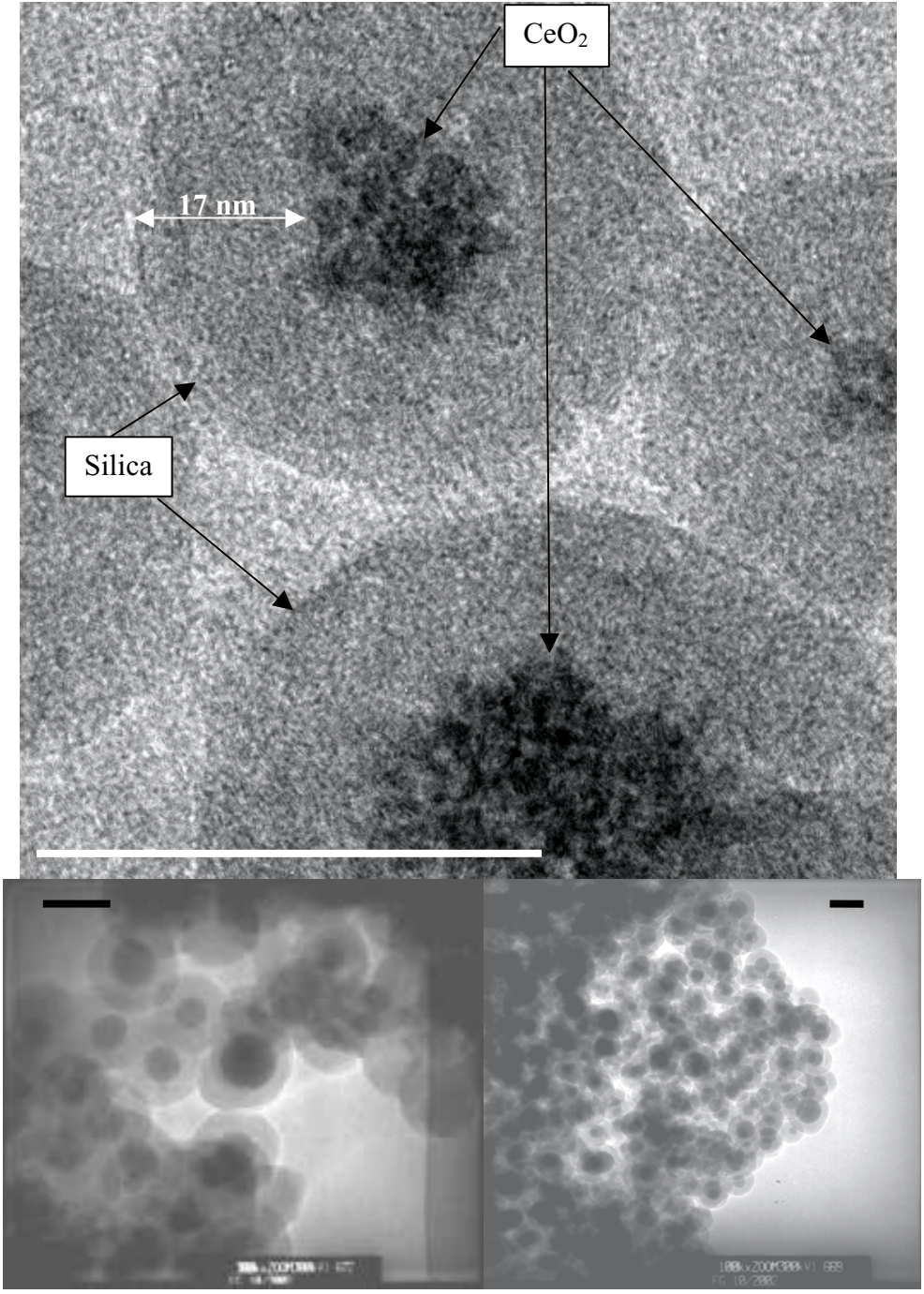

(All bars equal 50 nm)

Figure

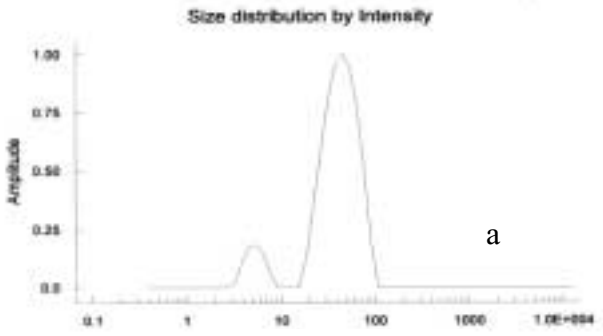

Diameter (nm)

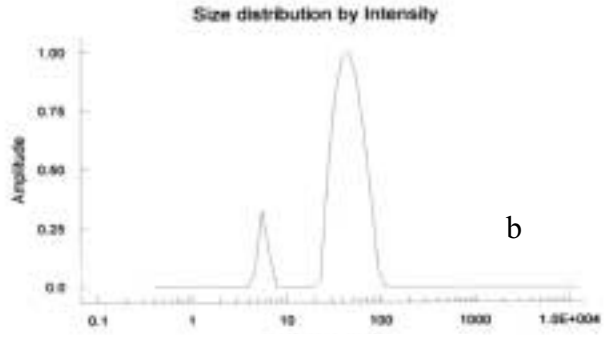

Diameter (nm)

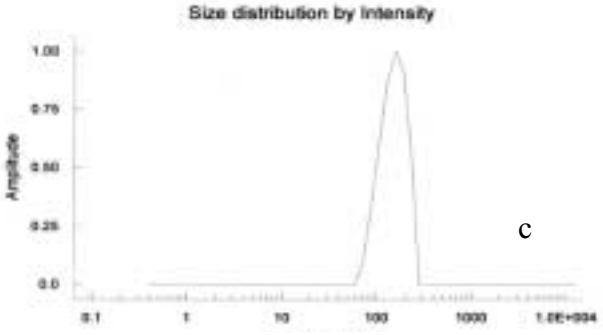

Diameter (nm)

Figure

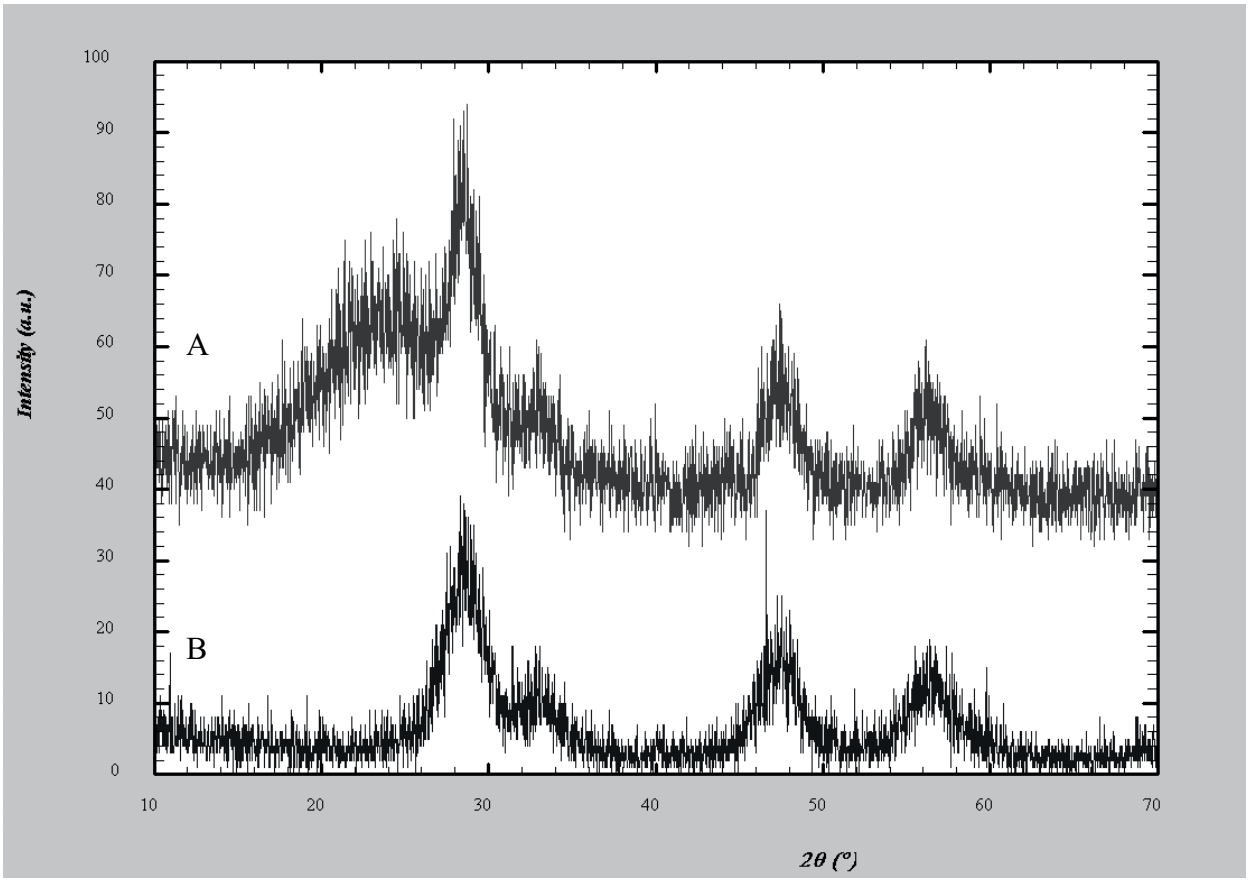
Intensity (a.u.)
2θ (°)
A
B
0
10
20
30
40
50
60
70
80
90
100
10
20
30
40
50
60
70

Figure

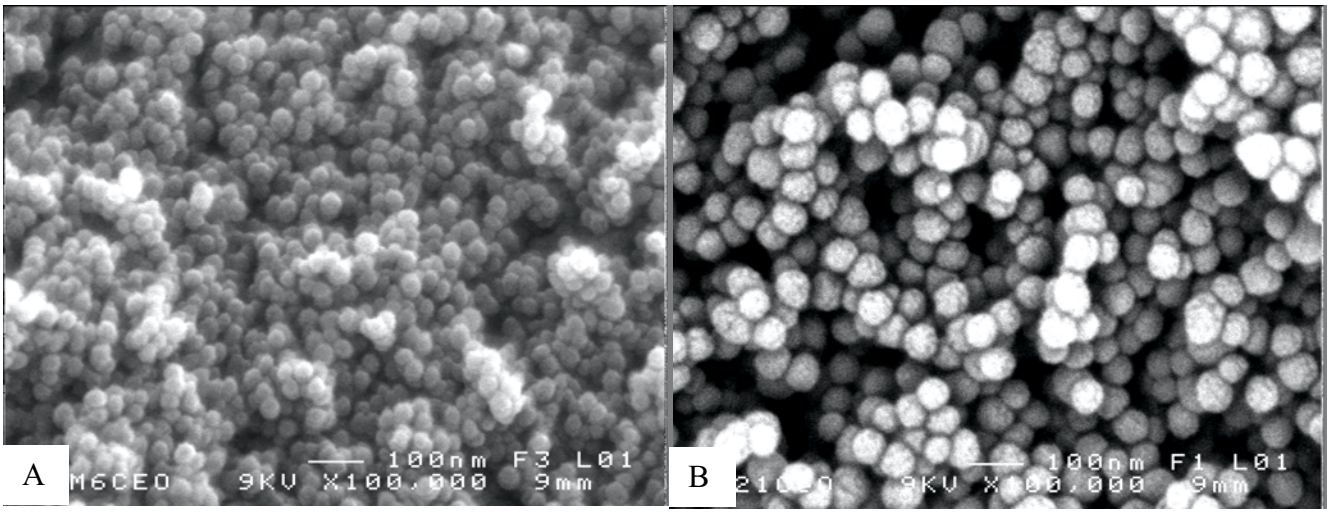
A
M6CE0 9KV X100,000 9mm
100nm F3 L01
B
9KV X100,000 9mm
100nm F1 L01

Figure